Cite this article as:
Tamburini A., Brucato A., Ciofalo M., Gagliano G., Micale G., Scargiali F., 2021, CFD simulations of early-to fully-turbulent conditions in unbaffled and baffled vessels stirred by a Rushton turbine, *Chemical Engineering Research and Design*, 171, 36-47. [10.1016/j.cherd.2021.04.021]

CFD SIMULATIONS OF EARLY- TO FULLY-TURBULENT CONDITIONS IN UNBAFFLED AND BAFFLED VESSELS STIRRED BY A RUSHTON TURBINE

Alessandro Tamburini, Alberto Brucato, Michele Ciofalo,

Gaetano Gagliano, Giorgio Micale, Francesca Scargiali*

Dipartimento di Ingegneria, Università di Palermo, Viale delle Scienze Ed. 6, 90128 Palermo (ITALY)

* Corresponding author: francesca.scargiali @unipa.it

Abstract. Laboratory scale unbaffled tanks provided with a top cover and a baffled tank both stirred by a Rushton turbine were simulated by carrying out RANS simulations. Three different turbulence models were adopted (*k-ω SST*, *k-ε* and the *SSG* Reynolds stress model) to predict the flow field and the relevant performance parameters (power and pumping numbers) of the tank operated from early to fully turbulent conditions. CFD results were compared with literature experimental data and DNS simulation results to validate and properly compare the models. In the range of Reynolds numbers investigated, results showed that, for the unbaffled tank, the *SSG* model based on Reynolds stresses is a better choice at larger Re, while the k-ω SST model better reproduces the experiments at lower values. Conversely, no significant differences between the predictions of the three models were found in the baffled vessel.

Keywords: stirred tank, unbaffled vessel, CFD, turbulence model, SSG.

1. INTRODUCTION

Mixing liquids in tanks provided with mechanical agitators is a common practice in process industry (Oldshue, 1983). Traditionally, most mixing operations have been carried out in baffled stirred vessels, thus leading to a large number of studies on this geometrical configuration (Bliatsiou et al., 2019; Carletti et al., 2018;-De Lamotte et al., 2018; Fan et al., 2018; He et al., 2019; Ljungqvist et al., 1998; Mousavi et al., 2019; Tamburini et al., 2009, 2012a). Conversely, the knowledge of unbaffled stirred tanks has been limited to the few applications in which the absence of baffles is compulsory or, at least, strongly recommended. Baffles are an intrinsic source of attrition and this could be a dramatic issue when delicate species such as living cells are to be mixed (Aloi and Cherry, 1996). Similarly, baffles may be an obstacle to flow and generate dead zones when high viscous fluids are to be mechanically agitated (Ameur et al., 2017; Chisti, 2000). These aspects are of crucial importance in bioreactors, crystallizers and pharmaceutical applications (Prakash et al., 2018; Busciglio et al., 2016; Hekmat et al., 2007; Brucato et al., 2017; Rotondi et al., 2021).

In the last years, interest is moving towards unbaffled vessels also for more traditional applications. For example, recent studies have shown that:

- some common mixing operations as the suspension of solid particles in liquids can be efficiently carried out in unbaffled vessels with large power savings (Tamburini et al., 2012b; Wang et al., 2012a,b; Tamburini et al., 2014; Wang et al., 2014);
- the presence of the central air-vortex (due to the highly swirling flow) can be exploited as a source of oxygen to be transferred to the solution (Cabaret et al., 2008; Tamburini et al., 2012b), with transfer rates comparable with those typical of baffled systems provided with an air-sparger (Tamburini et al., 2016; Labík et al., 2018; Scargiali et al., 2015);

- mixing times in unbaffled vessels may be comparable to baffled ones when the air vortex reaches the impeller depth (Busciglio et al., 2014);

Other commonly practical applications of unbaffled industrial tanks are the pigment dispersion by using radial flow high shear impellers in the paint and coating industries (Hockmeyer, 2010). In pigment dispersion processes with high shear impellers, the absence of baffles favours the vortex formation which helps to improve the incorporation time of floating pigments into the mixing solution (Ramírez-Gómez et al., 2015; Ramírez-Muñoz et al. 2016).

All of these recent outcomes are leading the number of studies on unbaffled vessels to increase. Many of them are devoted to investigating the vortex shape prediction along with the relevant gas-liquid hydrodynamics (Prakash et al., 2018; Deshpande et al., 2017; Nagata, 1975). Nagata (1975) was the first who proposed a simple model for the vortex shape prediction. Extension and modifications to this model have been proposed so far (Deshpande et al., 2017; Busciglio et al., 2013). Deshpande *et al.* adopted experimental and CFD investigation to extend Nagata's model to low Reynolds numbers (Deshpande et al., 2017). Prakash *et al.* studied the effect of impeller air ingestion on vortex shape at large Re (Prakash et al., 2018).

Other studies investigated different impeller types and configurations (Ameur et al., 2017; Yoshida et al., 2012; Zhang et al., 2018). Myers *et al.* (2011) studied the effect of tilting the shaft along with the impeller on the solid suspension features. Ameur *et al.* (2017) employed a radial impeller with elliptical blades for the mixing of a viscoplastic fluid. Recently, Zhang *et al.* (2018) proposed a novel cylindrical stirrer, which was found more efficient than the traditional Rushton and propeller agitators.

Although the number of studies is increasing, the understanding of unbaffled stirred tanks is still poor, while it is well known how much a full knowledge of these systems may be beneficial for a proper and efficient design. Moreover, the lack of a sufficient amount of studies and relevant information is another reason limiting the adoption of unbaffled tanks. In this regard, a full understanding of the key features of unbaffled tanks and of their key differences with

respect to baffled tanks may drive engineers towards the choice of the best configuration and operating conditions.

A number of different experimental techniques have been proposed so far to investigate stirred tanks. Laser Doppler Anemometry (*LDA*), Particle Image Velocimetry (*PIV*) and tomography are the most used (Hartmann et al., 2004; Martínez-Delgadillo et al., 2019; Sardeshpande et al., 2017). There are many other techniques available in the literature, but all of them have some limitations (Tamburini et al., 2013a): for instance, many of them are based on image analysis, thus intrinsically requiring the system to be transparent. Clearly, this may not be the case at an industrial level. Moreover, the amount of experiments to be carried out in order to collect a sufficient number of data at each operating condition (e.g. impeller velocity) is time-demanding. Computational Fluid Dynamics (CFD) is a powerful tool, which can significantly help to tackle this issue by collecting data and useful information at whatever level of detail (Janiga, 2019). Once a CFD model has been validated against purposely collected experimental data, much information can be derived from it at a fraction of the cost of experiments.

Several CFD simulations have been devoted to studying tanks provided with baffles, while this is not the case for unbaffled ones. Only a few applications of CFD to unbaffled stirred tanks are available in the literature (Trad et al., 2017; Li et al., 2017; Martínez-de Jesús et al., 2018; Li et al., 2020). Some of them are specifically devoted to the laminar regime where unbaffled tanks are largely used (Lamberto et al., 1999; Márquez-Baños et al., 2019; Guadarrama-Pérez et al., 2020), especially when non-Newtonian fluids are employed (Márquez-Baños et al., 2019; Guadarrama-Pérez et al., 2020). Others deal also with the turbulent regime (Glover and Fitzpatrick, 2007; Davoody et al., 2019). Glover and Fitzpatrick investigated via CFD modelling the vortex formation in an unbaffled stirred tank reactor (Glover and Fitzpatrick, 2007). Rotondi et al. (2021) made use of experiments and CFD simulations to test a novel bioreactor for improved cell and gene therapy applications. Davoody et al. (2019) investigated the scale formation in baffled and unbaffled tanks under turbulent regime by experimental and

modelling activities. Unsteady RANS were carried out to simulate the two tanks and unbaffled tanks were found to mitigate the scale formation more than baffled tanks in this regime.

Trad *et al.* (2017) investigated an anaerobic digester devoted to biohydrogen production and stirred by two different turbines placed at different shaft heights. Li *et al.* (2017) employed a CFD model based on a Reynolds stress model along with the Volume Of Fluid (VOF) approach to investigate a tank stirred by Pitched Blade Turbines (PBTs). Martinez de Jesus *et al.* (2018) carried out CFD simulations to analyse the performance of two novel high shear impellers. Ciofalo *et al.* (1996) performed numerical simulations of turbulent fluid flow in unbaffled tanks stirred by single-stage radial impellers using different Reynolds-averaged turbulence models. The results showed that only the use of a second-order Reynolds stress transport model allowed the correct prediction of the main flow characteristics, and, in particular, of radial profiles of the tangential velocity, whereas the k–ε model yielded an almost rigid-body motion with unphysical profiles of tangential velocity increasing monotonically from the rotation axis to the peripheral wall. Alcamo *et al.* (2005) performed Large-Eddy Simulation of Turbulent Flow in an Unbaffled Stirred Tank Driven by a Rushton Turbine.

However, none of the above studies has been explicitly devoted to recognizing the difference between baffled and unbaffled vessels at any fluid flow regime. In a previous work (Tamburini et al., 2018), our group performed Direct Numerical Simulations (*DNS*) to predict the velocity distribution and the relevant power and pumping number of both a baffled and an unbaffled lab-scale systems stirred at impeller speeds ranging from creeping to transitional or early turbulent flow conditions (Re≈1.7-600). The present work is aimed at extending such analysis from the transitional regime up to the achievement of fully turbulent conditions (Re≈600-33,000), a range of Reynolds numbers that has received little or no attention in the literature. The combination of low Re and swirling flow is in fact very difficult to simulate and represents a common source of failure for many turbulence models (Tamburini et al., 2018). Our purpose is

increasing the level of knowledge on how the flow field features of the two systems differentiate from steady conditions, where they are practically the same, to fully turbulent conditions, where they exhibit well known large differences.

2 VESSELS AND IMPELLER SPEEDS INVESTIGATED

Two lab-scale tanks were investigated, one baffled and the other unbaffled. Both had a diameter T equal to 0.19m and were filled with water up to a level H equal to T. A standard six bladed Rushton turbine was employed in the two vessels. Its diameter D was equal to $T/2$ and it was placed in both tanks at a distance C (clearance) from the vessel bottom equal to $T/3$. The two tanks, along with all the impeller features, are shown in Figure 1. A suitable cover was employed in the tanks in order to avoid the central air vortex typical of unbaffled vessels. The absence of a lid and the presence of the vortex would require specific treatment of the free surface, shadowing the influence of the turbulence model and making a comparison of the flow fields more cumbersome.

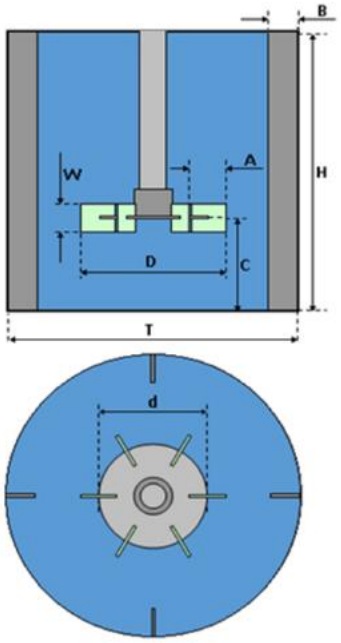

(A1)

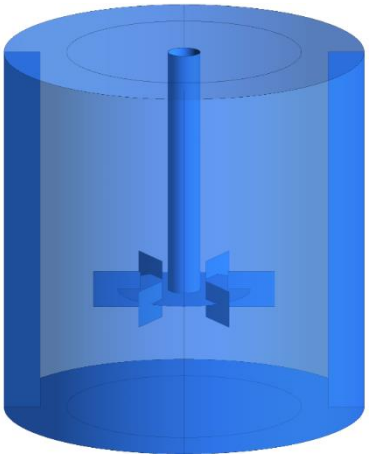

(A2)

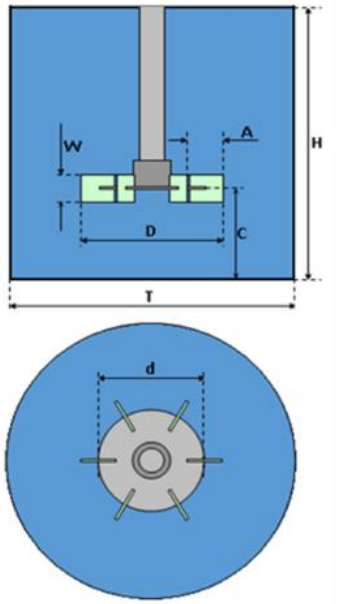

(B1)

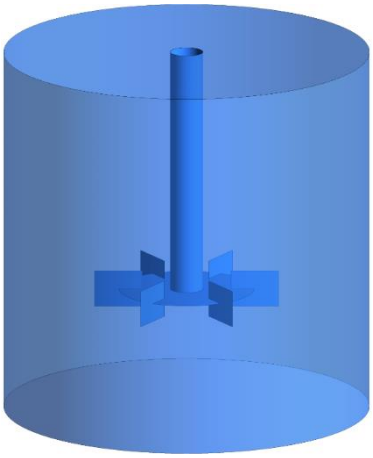

(B2)

T	***D***	***H***	***C***	***d***	***W***	***A***	***B***
---	*T*/2	*T*	*T*/3	3/4 *D*	*D*/5	*D*/4	*T*/10
0.19m	0.095m	0.19m	0.063m	0.07m	0.019m	0.0237m	0.019m

(C)

Figure 1: Sketch and features of the system investigated. A1) sketch of the baffled tank; A2) corresponding geometry built by the Ansys® software. B1) sketch of the unbaffled tank; B2) corresponding geometry built by the Ansys® software. C) geometrical features of the two tanks.

Several impeller speeds N were investigated. The corresponding Reynolds numbers ($Re=\rho ND^2/\mu$) are reported in Table 1: the highest Re corresponds to an impeller speed of about 200 RPM. The *Re* range under investigation encompasses early to fully turbulent conditions.

Table 1: Reynolds numbers simulated and CFD models compared.

Re	500	600	1000	2500	5000	10000	33000
DNS		Tamburini *et al.* (2018)					
k-ω SST	x	x	x	x	x	x	x
k-ε	x	x	x	x	x	x	x
SSG	x	x	x	x	x	x	x
LES							Alcamo *et al.* (2005)

3 MODELLING AND NUMERICAL DETAILS

3.1 Modelling

All simulations were performed by solving the continuity and momentum equations (Shaw, 1992) which are not reported here for the sake of brevity.

Given the aim of the present work, simulations were devoted to predicting the flow field in both tanks at Reynolds numbers corresponding to turbulent conditions for which DNS would be too computationally demanding. Thus, Reynolds averaging was performed for the continuity and momentum equations. Reynolds stresses were computed by adopting three different turbulence models:

- the *k-ε* turbulence model (Launder and Spalding, 1974);
- the *k-ω* Shear Stress Transport (*SST*) turbulence model (Wilcox, 1988; Menter et al., 2003);
- the Reynolds Stress turbulence model of Speziale, Sarkar and Gatski (*SSG*) (Launder et al., 1975).

The first two models are based on the Boussinesq hypothesis which accounts for a linear relationship between the Reynolds stresses and the first spatial derivatives of the time averaged velocities. The eddy viscosity is the coefficient of proportionality which is used for all the stresses. The k-ε model (Launder and Spalding, 1974) is probably still the most commonly used turbulence model, especially in the industrial sector. The model includes a transport equation for the turbulent kinetic energy k and one for the turbulent dissipation rate ε. The eddy viscosity is derived from k and ε via the Prandtl-Kolmogorov equation $\mu_t=\rho C_\mu k^2/\varepsilon$. The viscous sub-layer is not explicitly resolved by the model, rather, suitable wall functions are adopted to account for its effect. The k-ω *SST* model (Wilcox, 1988; Menter et al., 2003) is an evolution of the standard k-ω model which solves the two transport equations for the turbulence kinetic energy k and for the turbulence frequency ω ($\omega=\varepsilon/k$). The eddy viscosity is calculated from k and ω as $\mu_t=\rho k/\omega$. The k-ω *SST* model includes a blending function able to switch between the k-ε model in the free-stream and the k-ω model near the walls.

The *SSG* turbulence model does not adopt the Boussinesq hypothesis. It is an ε-based Reynolds stress model which includes 7 additional equations: six transport equations, one per each component of Reynolds stress tensor, and one transport equation for the turbulent dissipation rate ε. The *SSG* model shares the same equations of the more common Launder, Reece and Rodi (*LLR*) Reynolds stress model (Launder et al., 1975), but uses different values of the model constants; it has been found more accurate than *LRR* in many cases, in particular for swirling flows. Clearly, compared to an eddy viscosity model, a Reynolds stress model is intrinsically more complex and time-consuming. It includes more equations and the source terms are more complex to be accounted for. As a consequence, the model is less robust and convergence is more difficult to achieve.

All simulations were conducted by adopting the Ansys® CFX17.1 software (2017).

3.2 Numerical details

Concerning domain boundaries, these include vessel bottom, top-cover, lateral wall and baffles (*tank boundaries*), impeller blades, disk and shaft (*impeller boundaries*). All of them are considered as walls with no-slip boundary conditions. Zero thickness was assumed for the impeller boundaries and for the baffles. Clearly, baffles were included among the boundaries only for the baffled tank.

For the case of the unbaffled tank, all simulations were carried out in the frame of reference of the impeller. Thus, in this case, a counter-rotating velocity was fixed as a boundary condition on the tank side, bottom and top-cover walls, while no-slip boundary conditions were set for the impeller boundaries. Body forces accounting for centrifugal and Coriolis effects were added to the right-hand side of the momentum equations.

For the case of baffled systems, two alternative approaches were tested to account for the impeller-to-baffle relative rotation: (i) a transient and (ii) a stationary approach.

i) The transient approach requires the adoption of the Sliding Grid (SG) algorithm available in Ansys® CFX 17.1 with the *transient rotor-stator* option (Ansys, 2017). It requires the computational domain to be divided into two cylindrical, co-axial, non-overlapping sub-domains, as shown in Figure 2. The inner one includes the impeller and its computational grid rotates integrally with it, while the outer domain is stationary. The SG algorithm is used to allow for velocity and pressure data transfer from one domain to the other and vice versa. Note that the SG approach is intrinsically transient.

ii) The Multiple Reference Frame (MRF) approach is the stationary alternative to the sliding grid and it is very often used, especially for RANS simulations where steady-state conditions are investigated. Also in this case the tank is divided into two sub-domains: the inner one containing the impeller is simulated with the reference frame of the impeller itself, while the outer one including the baffles is simulated with the

laboratory reference frame. The flow field features relevant to these two domains are generally unsteady, but these are not much dependent on time and can be assumed stationary near a specific radial position (Luo et al. hypothesis (Luo et al., 1994)). When the surface of separation between the two domains is set close enough to this position, the flow field can be predicted by stationary simulations, thus guaranteeing lower computational times. With this respect, De La Concha-Gómez et al. (2019) investigated the effect of the position of this surface of separation on MRF simulation results. They found that this position does not affect the results in the laminar regime where the inner and outer flow are substantially uncoupled. Conversely, the separation position becomes important in the turbulent regime and should be moved at a larger radial position (i.e. more towards the periphery more), the higher the Reynolds number (De La Concha-Gómez et al., 2019).

If the surface of separation between the two domains is suitably chosen, MRF can provide results comparable with the more demanding transient SG ones, especially when global data predictions are looked for. For instance, regarding stirred tank reactors, reliable power requirements at the turbine shaft and turbine pumping capabilities can be obtained by MRF simulations. Conversely, in some cases, the transient SG treatment was found to provide better predictions when local data (such as velocity profiles) had to be predicted (Tamburini et al., 2013b). In addition, the use of transient simulations with SG approach is also particularly indicated when turbulent quantities as the turbulent kinetic energy and turbulent kinetic energy dissipation are to be predicted and for which MRF simulations have been found to provide less accurate results.

Clearly, larger computational times are required by the transient Sliding Grid approach. For the purpose of the present work, preliminary simulations were performed by adopting the transient approach at the minimum and maximum Reynolds number investigated and the predicted axial, radial and tangential velocity profiles were compared with corresponding ones obtained by

MRF steady-state simulations. The maximum discrepancy was found to be lower than 4% in all cases. Even lower differences (<2%) were found for the case of global output (e.g. power and pumping number) in accordance with the literature (Tamburini et al., 2011). Thus, only steady-state simulations via the MRF approach were carried out in the present work in order significantly to reduce the computational times.

Water at 25°C with density ρ=997 kg/m^3 and dynamic viscosity μ=8.899 10^{-4} kg/(m s) was used as the working fluid in all simulations. As mentioned above, the simulations were performed by adopting the finite volume based ANSYS® CFX 17.1 code (Ansys, 2017). It adopts a fully coupled algorithm to compute pressures and velocities by simultaneously solving the three hydrodynamics equations and the continuity equation. The Rhie and Chow (1982) discretization method for the mass flows is used in order to avoid the pressure field decoupling (Patankar, 1980). A multigrid technique is adopted for solving the discrete system of linearized equations. Variables are stored at the mesh nodes and shape functions are used to approximate the solution field or the solution gradients at integration points, as required by the evaluation of the various terms of the discretized transport equations. The high resolution (i.e. second-order upwind) scheme was adopted to discretize the advection terms. In preliminary transient simulations (using the sliding grid approach) the time derivatives of all variables were discretized by the second-order backward Euler scheme.

Steady-state simulations required by the RANS approach were performed by adopting a number of iterations sufficient to guarantee the normalized residuals of all variables to settle at values lower than 10^{-6}.

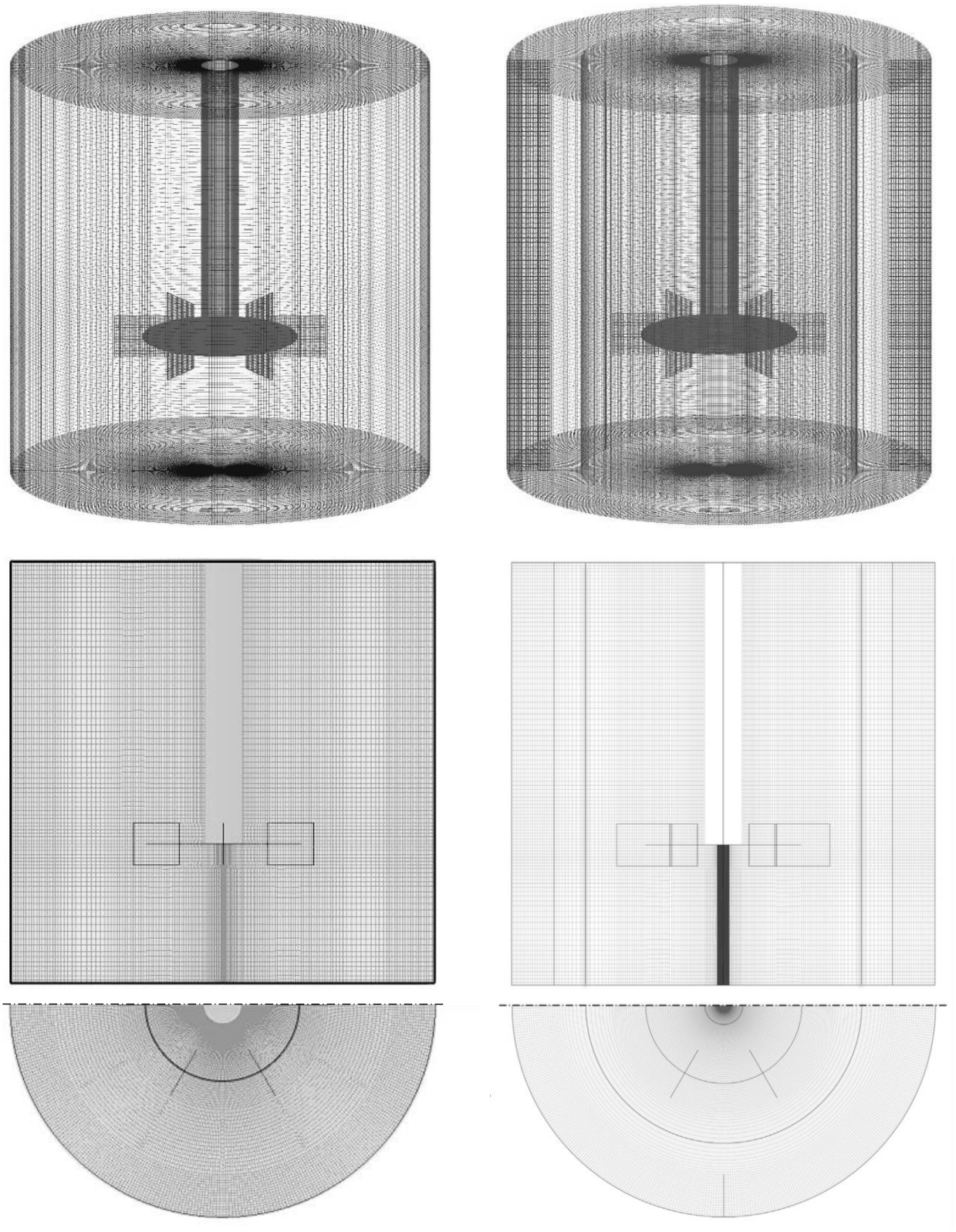

Figure 2: Computational grids employed. Left: unbaffled tank; right: baffled tank. The division into two co-axial sub-domains is shown for the baffled system.

Concerning the meshing, two block-structured grids were tested: a fine grid with about 5 million volumes and a very fine grid with 10 million volumes. For the case of the baffled system all grids were composed of two coaxial blocks (Figure 2), the inner one including the axis and the impeller, the outer one including the baffles. All of the grids were suitably refined near the impeller and solid walls, where the largest gradients are expected. Preliminary simulations were performed at the highest Re investigated in the present work (i.e. Re=33000) to evaluate the presence of any grid-dependence issue. This analysis concerned the comparison of both global quantities, such as the power and pumping number, and local data including local distributions of flow quantities such as the radial profiles of the axial and tangential velocities.

Regarding the global data, as it can be seen in Table 2, the relative error between the fine and the very fine grid was found lower than 3%.

Table 2: Grid dependence analysis. Comparison of $\boldsymbol{N_Q}$ and $\boldsymbol{N_p}$ data at the largest Re investigated (Re=33000). Data obtained by adopting the k-ω SST turbulence model.

	Fine Grid	Very fine Grid	Relative error [%]
N° finite volumes	4 753 240	9 957 456	---
Power Number N_p [-]	1.261	1.298	2.9%
Pumping Number N_Q [-]	0.340	0.348	2.4%

As far as the local data are concerned, Figure 3 shows azimuthally averaged radial profiles of the axial and tangential velocity at different heights from vessel bottom at Re = 33000 for the case of the unbaffled stirred tank. As clearly shown in the figure, very slight discrepancies can be recognized between the velocity component profiles obtained with the two grids. Identical profiles were found for the two grids for the case of the baffled vessel (not shown for the sake of brevity).

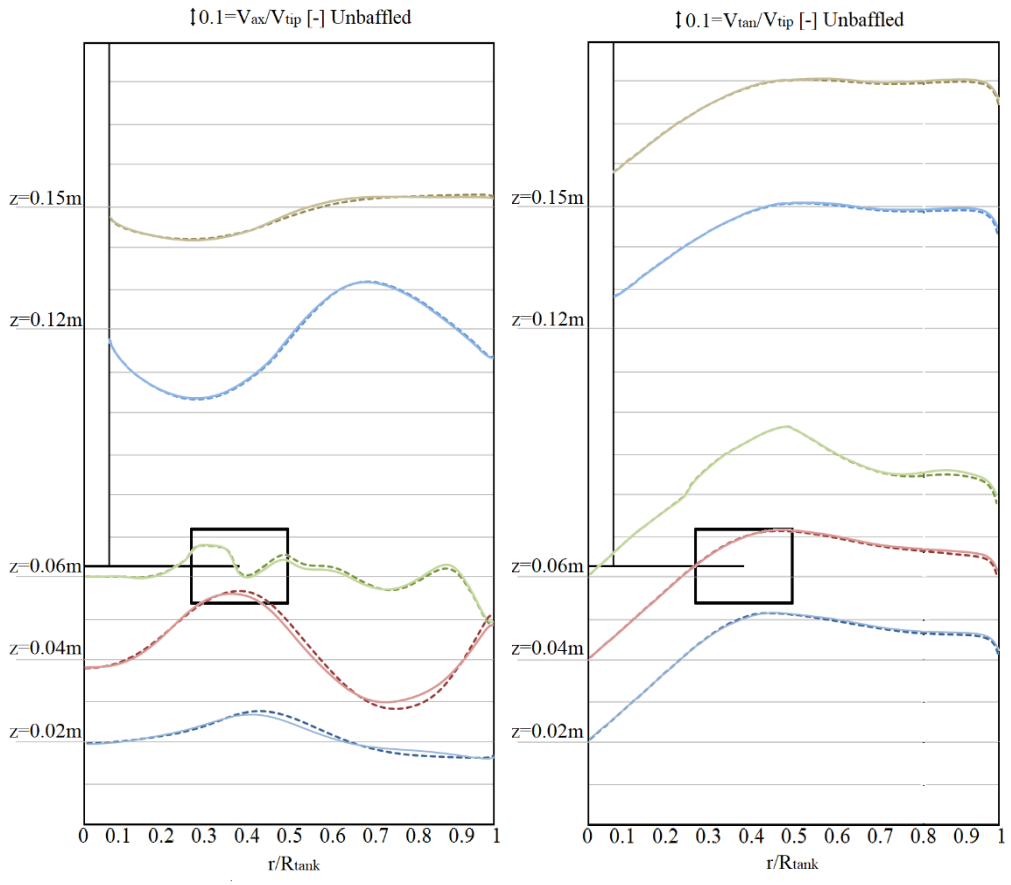

Figure 3: Azimuthally averaged radial profiles of the a) axial and b) tangential velocity at different heights from vessel bottom at Re= 33000 for the case of the unbaffled stirred tank. Continuous line: 4.75 million finite volumes; dotted line: 9.96 million finite volumes. Data obtained by adopting the k-ω SST turbulence model.

Collected data indicated that the mesh composed of 4.75 million finite volumes provides results very similar to those obtained with the very fine grid. Thus, the 4.75 million volume mesh, depicted in Figure 3, was adopted to carry out all the simulations.

4 RESULTS AND DISCUSSION

The present section is devoted to investigating the three different turbulence models tested by comparing them with one another and with corresponding experimental data. In order to do so, results are divided into two different categories: global and local data. Global data refer to performance parameters resulting from the complex interactions among velocities and

mechanical stresses arising in the tank and are of industrial interest. Local data refer to a lower scale and, in particular, concern local features of the flow field such as velocity profiles.

4.1 Global data

The pressure and flow field predicted as results of the CFD simulations are post-processed in order to provide global performance parameters. In particular, two parameters were calculated: the power number N_p and the pumping number N_Q:

$$N_P = \frac{P}{\rho N^3 D^5} \quad (1)$$

$$N_Q = \frac{Q}{ND^3} \quad (2)$$

where P is the power due to impeller+shaft torque and Q is the volumetric flow rate swept by the impeller (Oldshue, 1983).

The total torque was calculated by summing the single torques relevant to the rotating parts of the system (i.e. impeller disk, blades and shaft). Since the torque is totally transferred by the liquid to the motionless part of the tank, the torque power was also calculated by summing the torque values of all the still walls of the tank (i.e. bottom, cover, lateral wall and baffles for baffled tanks). Clearly, the two values should be identical: discrepancies always lower than 1.5% were found in the present simulations. The flow rate Q was computed by building a fictitious cylindrical surface surrounding the impeller blades (i.e. with a radius equal to the impeller one) in the software and calculating the volumetric flow rate exiting from it.

N_p values are reported in Figure 4 as functions of the Reynolds number. In order to compare the different turbulence model predictions, corresponding experimental data are reported in the same figure: in particular, data from Rushton *et al.* (1950) for baffled tanks and from Scargiali *et al.* (2017) for unbaffled tanks are reported. Also, N_p values predicted via DNS by Tamburini *et al.* (2018) are shown both for comparison purposes (at Re = 600) and for the sake of completeness. Finally, a LES N_p value by Alcamo *et al.* (2005), available for unbaffled tanks only, is also compared to the present simulations.

As far as the baffled tank is concerned, all three turbulence models provide very similar results in the whole range Re = 500~32,000. The well-known *plateau* of N_p at high Re, resulting from dimensional analysis and also shown by the experimental data, is very well predicted by all of the three turbulence models. For Re≥5000, also specific experimental values of N_p are well predicted. Conversely, a large overestimation of experimental values of N_p is found under very early turbulent conditions (Re=500-2500): thus, their adoption is not suggested in this range. This behaviour was somewhat unexpected for the *k-ω SST* turbulence model, which is commonly considered suitable for low-Re flows in which turbulence is not fully developed. Notably, the adoption of MRF approach in early turbulent conditions may be questionable for those cases where large instabilities may occur. DNS simulation results published in a previous paper (Tamburini et al., 2018) showed that this is not the case: at Re=600 turbulence was basically fully developed and no large instabilities were recognized. Moreover, a preliminary comparison of MRF and SG at Re=500 results in a discrepancy lower than 4%.

As regards the unbaffled tank, the decreasing trend of N_p with Re, similar to that of the friction factor in pipes, is predicted by all three turbulence models tested: the slope at early turbulent conditions is well predicted by the three models, while at fully turbulent conditions (commonly considered to be achieved at Re≥10,000) the experimental slope is steeper than the predicted ones. As a consequence, at very early turbulent conditions (Re≤1000) *k-ε* and *k-ω SST* results are very similar and in good agreement with experimental N_p values, while some underestimation is provided by the *SSG* Reynolds stress model. The opposite occurs at larger Reynolds numbers (Re=5000-32,000), where the best agreement is provided by the *SSG* turbulence model. Note that, in this range, *k-ε* and *k-ω SST* results bifurcate. Although, in some recent works, the *k-ω SST* model was reported to predict well the flow-field patterns at Re higher than those investigated here (7.1×10^4 in Zamiri and Chung, 2016), in the present work the agreement, at least on N_p, is good only for low-to-intermediate Re.

Summarizing, for *baffled* tanks all three models give comparable N_p predictions; they agree with experimental data at Re≥5000, but overpredict N_p at lower Re. For *unbaffled* tanks, the three models yield different N_p predictions; the best agreement with experimental data is provided by the *SSG* model for Re≥5000 and by the *k-ω SST* model at lower Re.

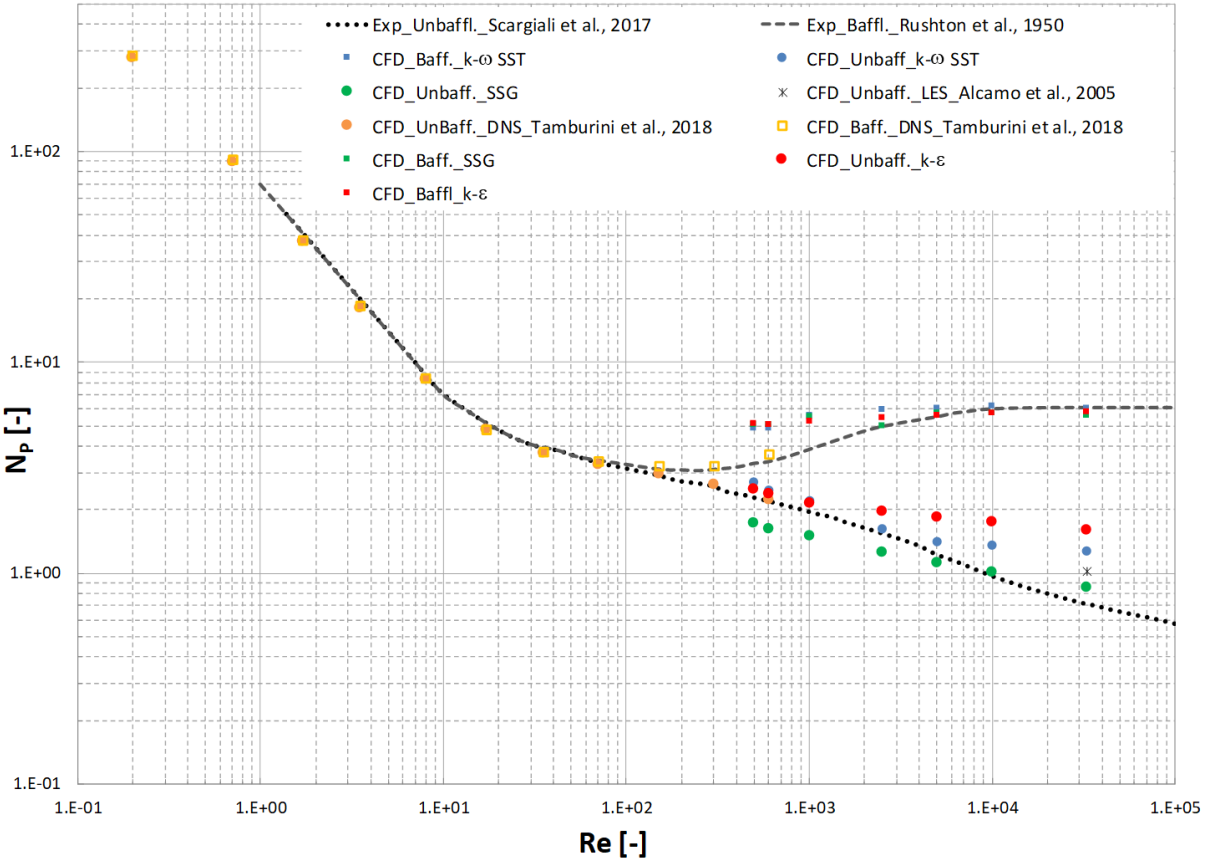

Figure 4: Power Number as a function of the Reynolds number: comparison between experiments and CFD simulations. Experimental data: broken lines. Baffled tank data: square points; Unbaffled tank data: circle points. *k-ω SST*: blue symbols; *k-ε*: red symbols; *SSG*: green symbols; DNS: orange symbols; LES: black star.

The values of the pumping number N_Q predicted by the turbulence models tested as functions of Re are shown in Figure 5. These data are reported along with N_Q values predicted by DNS simulations (Tamburini et al., 2018) at low *Re* for the sake of completeness. For this quantity, literature experimental data are available only at fully turbulent conditions: a N_Q of about 0.73 was measured by Costes and Couderc (1988) for baffled tanks, while Nagata (1975) reported a value of about 0.34 for unbaffled vessels. These values should be regarded as purely asymptotic:

in particular, the one relevant to the baffled vessel should be seen as the limiting value of the N_Q vs Re sigmoidal trend theoretically predicted by Dickey and Fenic (1976).

For the baffled tank, the right-end of this trend is well predicted by all three turbulence models, while, for the transition from the last DNS result (~0.62 at Re=600) to the high-Re value of ~0.78-0.80, the three models give different and somewhat puzzling results. In particular, all models overpredict N_Q with respect to DNS for Re=600; *SSG* results exhibits a strong increase of N_Q around Re=1000; and k-ε results show a decreasing N_Q between Re=500 and 600. Clearly, the above model comparison should be regarded as mainly qualitative given the lack of experimental or DNS data at all the intermediate Re investigated here.

In regard to the unbaffled tank, the three models exhibit a similar N_Q vs Re slope and a similar trend. The best agreement with DNS results in the small Re interval of overlapping is provided by the k-ε model, while SSG results are some 20% lower. None of the models clearly exhibits an asymptotic trend, at least within the range of Re investigated.

A comparison of Figures 4 and 5 indicates that the higher pumping capability of the impeller typical of baffled tanks should be properly compared with the corresponding power drawn which is higher as well. Only a comparison based on an economic analysis suitably tailored to a specific process may allow recognizing which tank option may be more convenient.

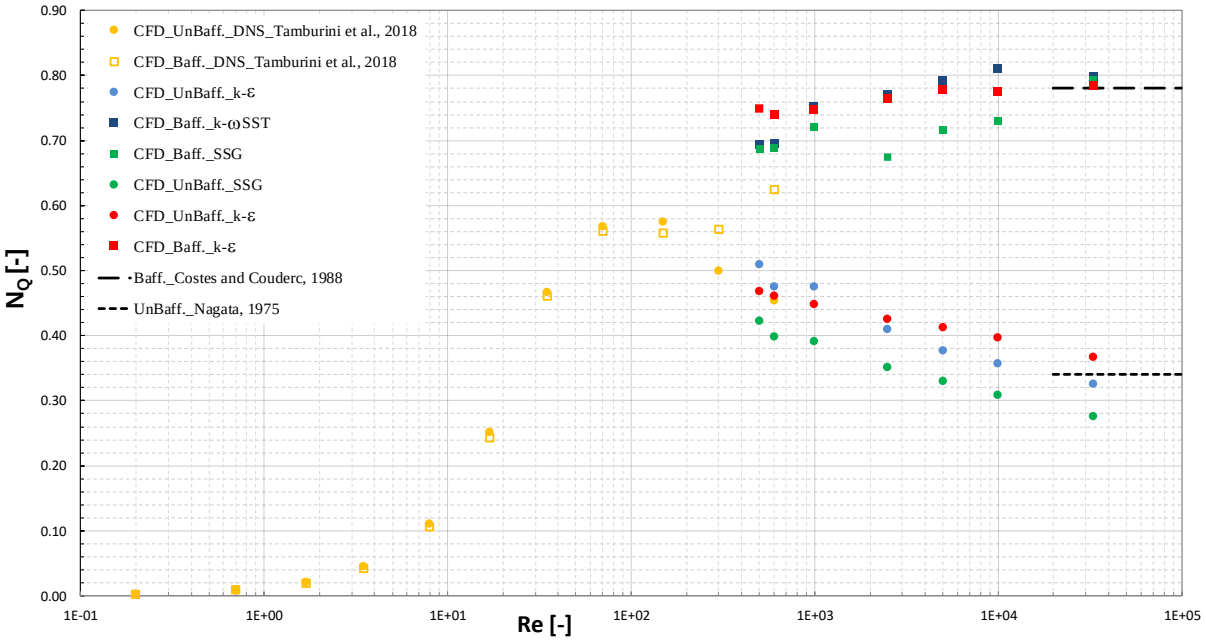

Figure 5: Pumping Number as a function of the Reynolds number. Comparison between literature data and CFD simulations. Literature data: broken lines. Baffled tank data: squares; Unbaffled tank data: circles. *k-ω SST*: blue symbols; *k-ε*: red symbols; *SSG*: green symbols; DNS: orange symbols.

4.2 Local data

Different models can predict similar global data even if different flow fields are calculated (Tamburini et al., 2011). The comparison among the turbulence model predictions was also extended to local data. In particular, Figure 6 shows azimuthally averaged radial profiles of the tangential velocity (normalized by $v_{tip}=ND/2$) at Re=33,000 for the case of the unbaffled vessel. Experimental data and corresponding LES predictions by Alcamo *et al.* (2005) are also reported for comparison purposes. As it can be seen, all the models are found able to predict correctly the linear trend (typical of rigid body rotation) up to a radial position somehow corresponding to the impeller diameter. At larger radii, predictions from LES and from the *SSG* turbulence model are in good agreement with the experimental trend, while the high swirling flow at this Re leads both eddy-viscosity models to overestimate the tangential velocities (more severely for the *k-ε*). The local results of Figure 6 are consistent with the outcome of Figure 4 for the global parameter N_p and suggest that, at very large Re, only a reliable description of the

turbulence anisotropy can lead to a good agreement with experimental data. This is in accordance with the outcomes of Argyropoulos and Markatos (2015), who tested a number of turbulence models for some practical applications.

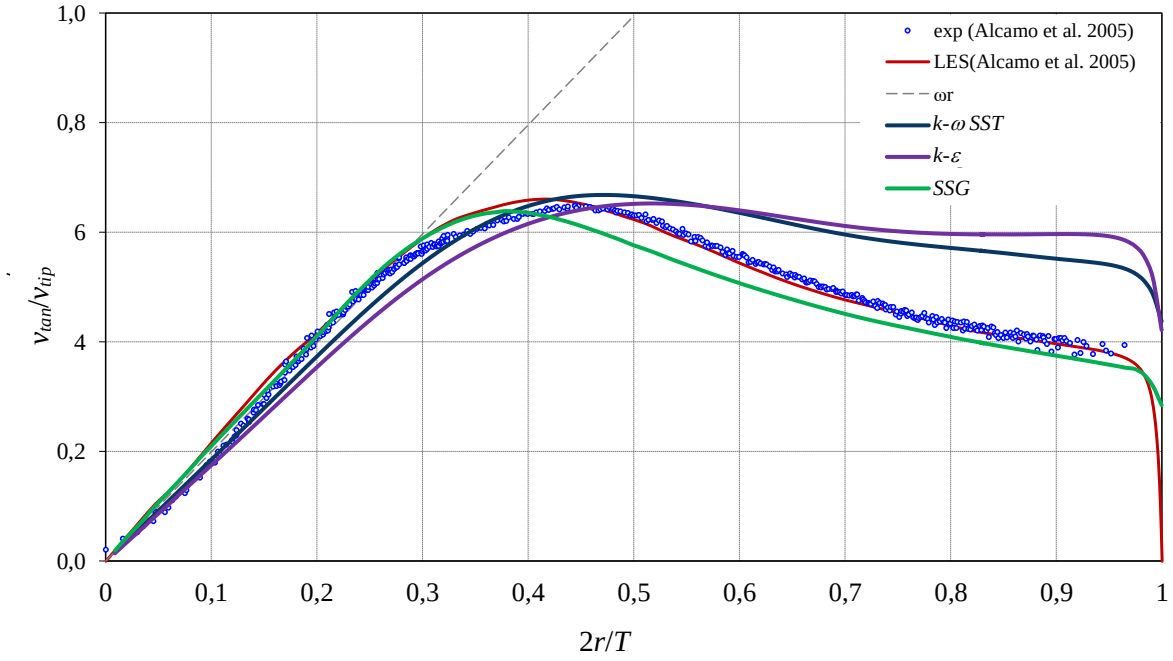

Figure 6: Unbaffled tank: azimuthally averaged radial profiles of the tangential velocity at z=4cm from vessel bottom at Re= 33000. Profiles are normalized by v_{tip}.

Azimuthally averaged radial profiles of the axial and tangential velocity (both normalized by v_{tip}) at different heights from vessel bottom at Re = 600 are shown in Figure 7. As regards the unbaffled tank, among the three turbulence models tested, the velocity profiles (both axial and tangential) predicted by the *k-ω SST* are the closest to the DNS predictions. The *SSG* fails in following the DNS profiles, especially the tangential velocity ones, thus confirming the finding of Figure 4 and suggesting not to adopt it at very early turbulent conditions. A similar disagreement was found for the *k-ε* model which, in particular, provides even worse tangential velocities at planes above the impeller. The best performance of the *k-ω SST* model can be also inferred from the countour maps and vector plots on a vertical diametral plane shown in Figure 8: both the axial and the tangential velocity predicted by the *k-ω SST* model are the most similar to the DNS ones.

Concerning the baffled tank, the DNS axial velocities shown in Figure 7 and in Figure 9 are well predicted by the three turbulence models, at any plane height. Conversely, only a fair agreement is found for the tangential velocities. With reference to Figure 7, among the three models, the *k-ω SST* predictions seem closer to the DNS ones: even opposite tangential velocities are provided by the *k-ε* at radial positions lower than the impeller radius. Interestingly, predictions similar and quantitatively close to DNS are provided by the three models near the impeller plane where the largest turbulence anisotropy occurs.

Comparing the two tanks, the axial velocity components are found quantitatively very similar at planes over the impeller, while they are higher in the baffled tanks below the impeller being the impeller clearance lower than *T*/2. This is not the case for the tangential velocities, which are higher in the unbaffled vessel at any plane as expected.

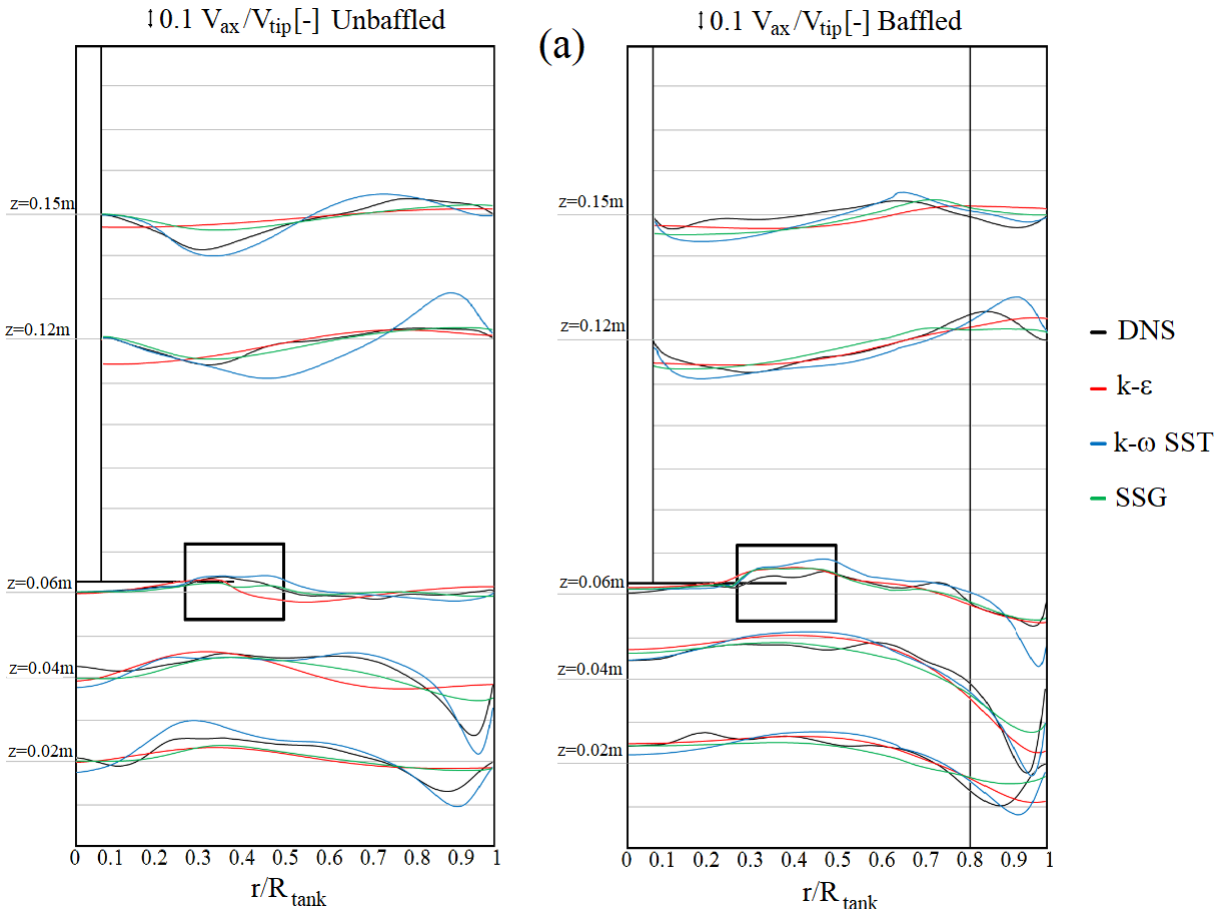

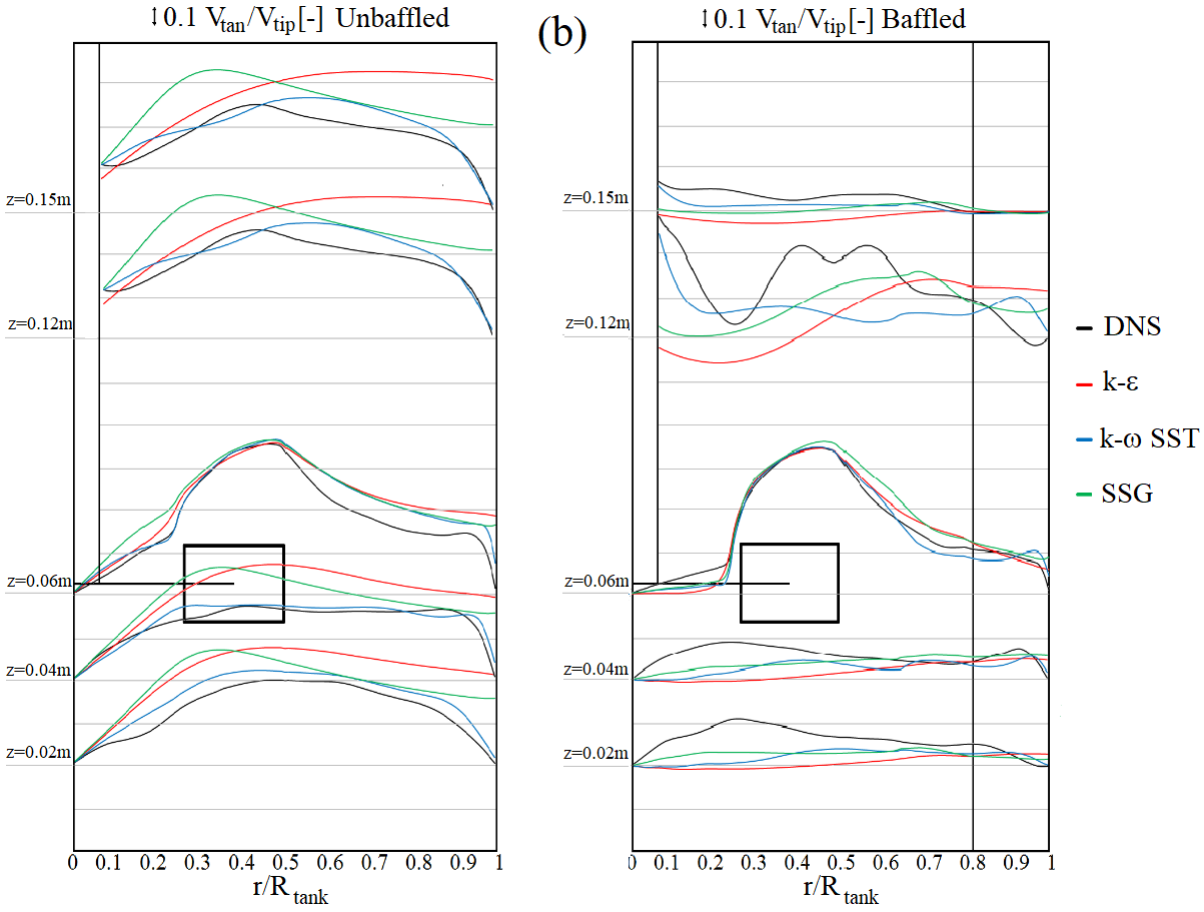

Figure 7: Azimuthally averaged radial profiles of the a) axial and b) tangential velocity at different heights from vessel bottom at Re= 600. Left: unbaffled tank. Right: baffled tank.

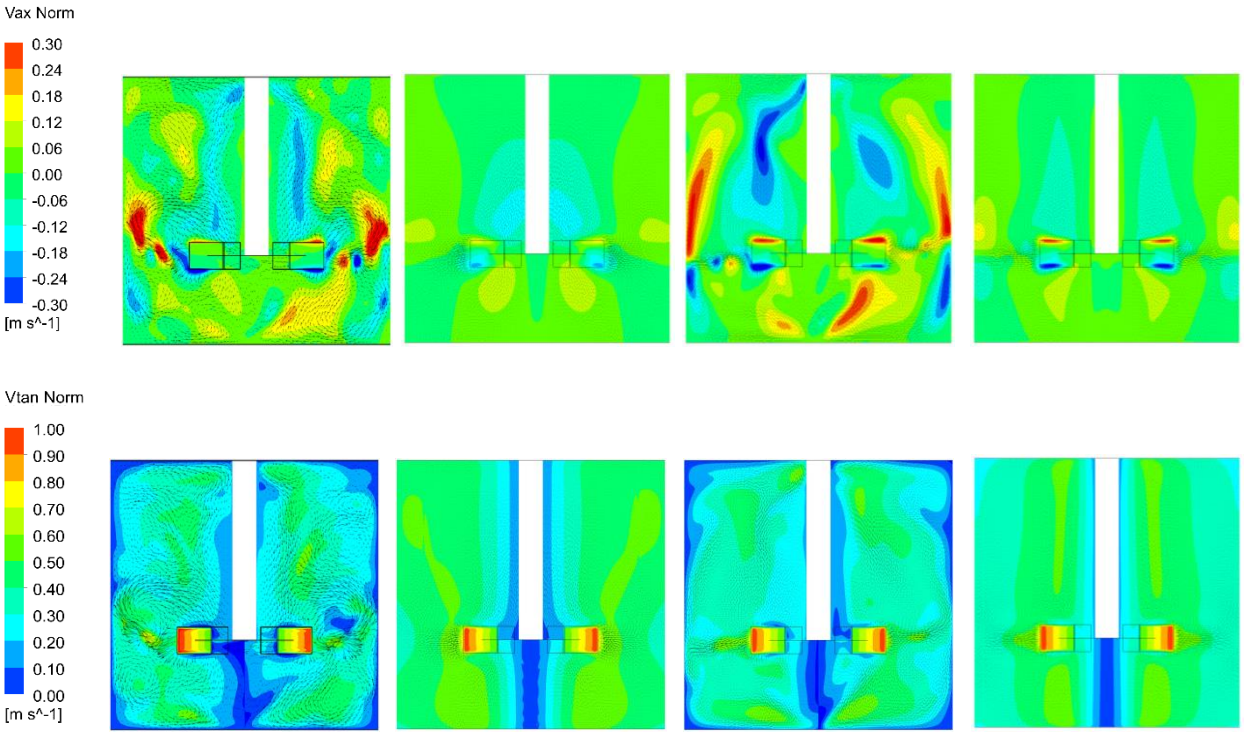

Figure 8: False colour maps and vector plots of axial v_{ax} (upper row) and tangential v_{tan} (lower row) velocity components (normalized by $_{vtip}$) in the unbaffled tank. (a) DNS; (b) k-ε; (c) k-ω SST; (d) SSG.

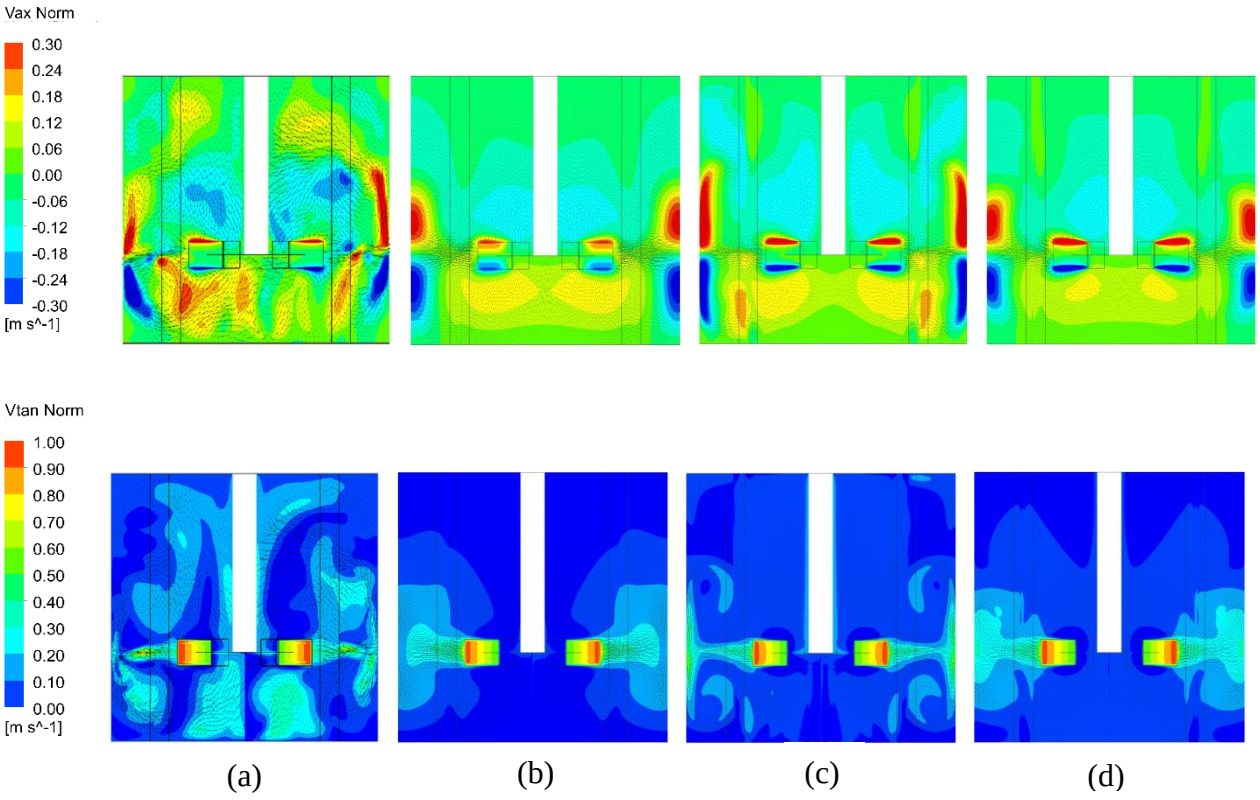

Figure 9: False colour maps and vector plots of axial v_{ax} (upper row) and tangential v_{tan} (lower row) velocity components (normalized by $_{vtip}$) in the baffled tank. (a) DNS; (b) k-ε; (c) k-ω SST; (d) SSG.

5. CONCLUSIONS

The present work compares for the first time the predictions capability of different RANS turbulence models (*k-ω SST*, *k-ε* and *SSG*) in baffled and unbaffled tanks operated at Reynolds numbers ranging from early- to fully-turbulent conditions. Both global quantities (power and pumping numbers N_p, N_Q) and local data (azimuthally averaged radial profiles of axial and tangential velocities) were predicted and results were compared with literature data encompassing experimental and computational (*DNS* and *LES*) results.

Concerning the baffled tank, all the models' predictions were found in agreement with the experimental data at large Re (fully turbulent flow) while at lower Re (transitional and early-turbulent flow) some disagreement was found. Among the three models, the *k-ω SST* was the best option at low *Re*, while tangential velocities even opposite than the DNS ones were predicted by the *k-ε* model.

In regard to the unbaffled vessel, reliable predictions were provided by the *k-ω SST* model in the lower Re range (500-2500), while, at larger Re, the *SSG* turbulence model was the only one able to provide satisfactory prediction of both local and global data.

In all cases, the *k-ω SST* was found better than the *k-ε* at the Reynolds numbers investigated, thus indicating that a fine resolution of the near-wall layer is crucial to get sound results under early turbulent conditions.

On the whole, according to the findings of the present works, the *k-ω SST* appears reliable enough to predict the flow-field local and global features of both baffled and unbaffled vessel and should be regarded as the reference turbulence model for low computationally-demanding simulations (within the *Re* range investigated). The adoption of LES or Reynolds stress models (such as the *SSG*) should be considered preferable in unbaffled vessels at high Re (fully turbulent conditions).

NOTATION

A	impeller blade width (m)
B	baffle width (m)
C	impeller clearance (m)
C_μ	Prandtl-Kolmogorov equation constant (-)
D	impeller diameter (m)
b	disk diameter (m)
H	liquid height (m)
k	turbulent kinetic energy (m^2/s^2)
N	rotational impeller speed (rpm)
N_p	power number (-)
N_Q	pumping number (-)
P	power (Watt)
Q	Flow rate discharged by the impeller (m^3/s)
r	radial coordinate, (m)
R_{tank}	tank radius (m)
Re	Reynolds number (-)
T	tank diameter (m)
v	mean velocity (m/s)
W	impeller blade height (m)
z	axial coordinate (m)

Greek letters

ε	turbulent dissipation rate (W/kg)
μ	viscosity (Pa s)
ρ	density (kg m^{-3})
ω	turbulence frequency (1/s)

Subscripts

ax	axial
t	turbulent
tan	tangential
tip	impeller blade tip

REFERENCES

Alcamo R., Micale G., Grisafi F., Brucato A., and Ciofalo M., 2005. “Large-eddy simulation of turbulent flow in an unbaffled stirred tank driven by a Rushton turbine,” Chem. Eng. Sci., vol. 60, no. 8–9, pp. 2303–2316.

Ameur H., Sahel D., and Kamla Y., 2017. “Energy efficiency of a deep hollow bladed impeller for mixing viscoplastic fluids in a cylindrical vessel,” Adv. Mech. Eng., vol. 9, no. 5, pp. 1–7.

Ansys Inc., “Ansys-CFX Reference Guide,” Release 18.0, vol. I,

Argyropoulos C. D. and Markatos N. C., 2015. “Recent advances on the numerical modelling of turbulent flows,” Appl. Math. Model., vol. 39, no. 2, pp. 693–732.

Bliatsiou C., Malik A., Böhm L., and Kraume M., 2019. “Influence of Impeller Geometry on Hydromechanical Stress in Stirred Liquid/Liquid Dispersions,” Ind. Eng. Chem. Res., vol. 58, no. 7, pp. 2537–2550.

Busciglio A., Caputo G., and Scargiali F., 2013. “Free-surface shape in unbaffled stirred vessels: Experimental study via digital image analysis,” Chem. Eng. Sci., vol. 104, pp. 868–880.

Busciglio A., Grisafi F., Scargiali F. and Brucato A., 2014. “Mixing dynamics in uncovered unbaffled stirred tanks,” Chem. Eng. J., vol. 254, pp. 210–219.

Busciglio A., Scargiali F., Grisafi F., and A. Brucato, 2016. “Oscillation dynamics of free vortex surface in uncovered unbaffled stirred vessels,” Chem. Eng. J., vol. 285, pp. 477–486.

Brucato A., Busciglio A., and Scargiali F., 2017. “Unbaffled, Stirred Bioreactors for Animal Cell Cultivation,” in Current Developments in Biotechnology and Bioengineering, Elsevier, pp. 97–142.

Cabaret F., Fradette L., and Tanguy P. A., 2008. “Gas–liquid mass transfer in unbaffled dual-impeller mixers,” Chem. Eng. Sci., vol. 63, no. 6, pp. 1636–1647.

Carletti C., Bikić S., Montante G., and Paglianti A., 2018. “Mass Transfer in Dilute Solid–Liquid Stirred Tanks,” Ind. Eng. Chem. Res., vol. 57, no. 18, pp. 6505–6515.

Chisti Y., 2000. “Animal-cell damage in sparged bioreactors,” Trends Biotechnol., vol. 18, no. 10, pp. 420–432.

Ciofalo M., Brucato A., Grisafi F., Torraca N., 1996. Turbulent Fluid Flow in Closed- and Free-Surface Unbaffled Tanks Stirred by Radial Impellers, Chemical Engineering Science, Vol. 51, No. 14, pp. 3557-3573.

Costes J. and Couderc J. P., 1988. Study by laser Doppler anemometry of the turbulent flow induced by a Rushton turbine in a stirred tank: Influence of the size of the units-I. Mean flow and turbulence. Chem. Eng. Sci., 43 (10) 2751–2764.

Davoody, M., Graham, L.J.W., Wu, J., Witt, P.J., 2019. Madapusi, S., Parthasarathy, R., Mitigation of scale formation in unbaffled stirred tanks-experimental assessment and quantification. Chemical Engineering Research and Design, 146, 11-21.

De La Concha-Gómez, A.D., Ramírez-Muñoz, J., Márquez-Baños, V.E., Haro, C., Alonso-Gómez, A.R. 2019. Effect of the rotating reference frame size for simulating a mixing straight-blade impeller in a baffled stirred tank. Revista Mexicana de Ingeniera Quimica, 18(3), 1143-1160.

De Lamotte A., Delafosse A., Calvo S., and Toye D., 2018. “Identifying dominant spatial and time characteristics of flow dynamics within free-surface baffled stirred-tanks from CFD simulations,” Chem. Eng. Sci., vol. 192, pp. 128–142.

Deshpande S. S., Kar K. K., Walker J., Pressler J., and Su W., “An experimental and computational investigation of vortex formation in an unbaffled stirred tank,” Chem. Eng. Sci., vol. 168, pp. 495–506, 2017.

Dickey, D., Fenic, J. C., Dimensional analysis for fluid agitation systems. Chem. Eng., 83 (1976) 139–145.

Fan W., Yuan L., and Qu X., 2018. “CFD simulation of hydrodynamic behaviors and aerobic sludge granulation in a stirred tank with lower ratio of height to diameter,” Biochem. Eng. J., vol. 137, pp. 78–94.

Glover, G. M. C., Fitzpatrick, J. J., 2007. Modelling vortex formation in an unbaffled stirred tank reactors. Chemical Engineering Journal 127, 11-22.

Guadarrama-Pérez, R., Márquez-Baños, V.E., De La Concha-Gómez, A.D., Valencia-López, J.J., Vengoechea-Pimienta, A., Martínez de Jesús, G., Ramírez-Muñoz, J., 2020. Hydrodynamic Performance of a Ring-Style High-Shear Impeller in Newtonian and Shear-Thinning Fluids. Chemical Engineering and Technology 43, 2325-2335.

Hartmann H., Derksen J. J., Montavon C., Pearson J., Hamill I. S., and Van den Akker H. E. A., 2004. “Assessment of large eddy and RANS stirred tank simulations by means of LDA,” Chem. Eng. Sci., vol. 59, no. 12, pp. 2419–2432.

He W., Xie Z., Zhao Z., Huang M., and Pan M., 2019. “Effect of impeller clearance on floc growth behaviors in a baffled square stirred-tank reactor: Flocculation-test and CFD-aided studies,” Sep. Purif. Technol., vol. 212, pp. 233–244.

Hekmat D., Hebel D., Schmid H., and Weuster-Botz D., 2007. “Crystallization of lysozyme: From vapor diffusion experiments to batch crystallization in agitated ml-scale vessels,” Process Biochem., vol. 42, no. 12, pp. 1649–1654.

Hockmeyer, H., 2010. A practical guide to high-speed dispersion, Paint Coat. Ind., 26, 32–36.

Janiga G., 2019. “Large-eddy simulation and 3D proper orthogonal decomposition of the hydrodynamics in a stirred tank,” Chem. Eng. Sci., vol. 201, pp. 132–144.

Labík L., Petricek R., Moucha T., Brucato A., Caputo G., Grisafi F., Scargiali F., 2018. “Scale-up and viscosity effects on gas–liquid mass transfer rates in unbaffled stirred tanks,” Chem. Eng. Res. Des., vol. 132, pp. 584–592.

Lamberto, D.J., Alvarez, M.M., Muzzio, F.J., 1999. Experimental and computational investigation of the laminar flow structure in a stirred tank, Chemical Engineering Science 54, 919-942.

Launder B. E. and Spalding D. B., 1974. “The numerical computation of turbulent flows,” Comput. Methods Appl. Mech. Eng., vol. 3, no. 2, pp. 269–289.

Launder B. E., Reece G. J., and Rodi W., 1975. “Progress in the development of a Reynolds-stress turbulence closure,” J. Fluid Mech., vol. 68, no. 3, pp. 537–566.

Li L., Wang J., Feng L., and Gu X., 2017. “Computational fluid dynamics simulation of hydrodynamics in an uncovered unbaffled tank agitated by pitched blade turbines,” Korean J. Chem. Eng., vol. 34, no. 11, pp. 2811–2822.

Li, L., Xiang, K., Xiang, B., 2020. Numerical simulation of transient power consumption characteristics in an unbaffled stirred tank. Chemical Papers 74, 2849-2859.

Ljungqvist M. and Rasmuson A., 1998. A comparison of the hydrodynamics of open and closed stirred vessels. Chem. Eng. Commun., vol. 165, no. 1, pp. 123–150.

Luo J. Y., Issa R. I., and Gosman A. D., 1994. Prediction of impeller induced flows in mixing vessels using multiple frames of reference, in 8th European conference on mixing, pp. 549–556.

Márquez-Baños, V.E., De La Concha-Gómez, A.D., Valencia-López, J.J., López-Yáñez, A., Ramírez-Muñoz, J., 2019. Shear rate and direct numerical calculation of the Metzner-Otto constant for a pitched blade turbine. Journal of Food Engineering 257, 10-18.

Martínez-de Jesús G., Ramírez-Muñoz J., García-Cortés D., and Cota L. G., 2018. "Computational Fluid Dynamics Study of Flow Induced by a Grooved High-Shear Impeller in an Unbaffled Tank," Chem. Eng. Technol., vol. 41, no. 3, pp. 580–589.

Martínez-Delgadillo S. A., Alonzo-Garcia A., Mendoza-Escamilla V. X., González-Neria I., and Antonio Yáñez-Varela J., 2019. "Analysis of the turbulent flow and trailing vortices induced by new design grooved blade impellers in a baffled tank," Chem. Eng. J., vol. 358, pp. 225–235.

Menter F. R., Kuntz M., and Langtry R. B., 2003. "Ten years of industrial experience with the SST turbulence model," in Turbulence, heat and mass transfer 4 : proceedings of the Fourth International Symposium on Turbulence, Heat and Mass Transfer, pp. 1–8.

Mousavi S. E., Choudhury M. R., and Rahaman M. S., 2019. "3-D CFD-PBM coupled modeling and experimental investigation of struvite precipitation in a batch stirred reactor," Chem. Eng. J., vol. 361, pp. 690–702.

Myers K. J., Herr J. P., and Janz E. E., 2011. "Solids suspension with angle-mounted agitators in unbaffled vessels," Can. J. Chem. Eng., vol. 89, no. 4, pp. 940–947.

Nagata S., Mixing – Principles and Applications. New York: Wiley, 1975.

Oldshue J. Y., Fluid Mixing Technology. New York: Chem. Eng. McGraw-Hill Pub., 1983.

Patankar S. V., Numerical heat transfer and fluid flow. Washington, DC,: Hemisphere Publishing Corp, 1980.

Prakash B., Bhatelia T., Wadnerkar D., Shah M. T., Pareek V. K., and Utikar R. P., 2018. "Vortex Shape and Gas-Liquid Hydrodynamics in Unbaffled Stirred Tank," Can. J. Chem. Eng., vol. 9999, pp. 1–8.

Ramírez-Gómez, R., García-Cortés, D., Martínez-de Jesús, G., González-Brambila, M.M., Alonso, A., Martínez-Delgadillo, S.A., Ramírez-Muñoz, J., 2015. Performance evaluation of two high-shear impellers in an unbaffled stirred tank, Chem. Eng. Technol., 38, 1519–1529.

Ramírez-Muñoz, J., Martínez-de-Jesús, G., Soria, A., Alonso, A., Torres, L.G., 2016. Assessment of the effective viscous dissipation for deagglomeration processes induced by a high shear impeller in a stirred tank. Advanced Powder Technology, 27, 1885–1897.

Rhie C. M. and Chow W. L., 1982. "Numerical study of the turbulent flow past an airfoil with trailing edge separation," in AIAA/ASME 3rd Joint Thermophysics, Fluids, Plasma and Heat Transfer Conference, p. 12.

Rotondi, M., Grace, N., Betts, J., Bargh, N., Costariol, E., Zoro, B., Hewitt, C.J., Nienow, A.W., Rafiq, Q.A., 2021. Design and development of a new ambr250® bioreactor vessel for improved cell and gene therapy applications. Biotechnology Letters – in press. 10.1007/s10529-021-03076-3.

Rushton J. H., Costich E. W., and Everett H. J., 1950. “Power characteristics of mixing impeller - Part I,” Chem. Eng. Prog., vol. 46, pp. 395–403.

Sardeshpande M. V., Gupta S., and Ranade V. V., 2017. “Electrical resistance tomography for gas holdup in a gas-liquid stirred tank reactor,” Chem. Eng. Sci., vol. 170, pp. 476–490.

Scargiali F., Busciglio A., Grisafi F., and Brucato A., 2015. “Free surface oxygen transfer in large aspect ratio unbaffled bio-reactors, with or without draft-tube,” Biochem. Eng. J., vol. 100, pp. 16–22.

Scargiali F., Tamburini A., Caputo G., and Micale G., 2017. “On the assessment of power consumption and critical impeller speed in vortexing unbaffled stirred tanks,” Chem. Eng. Res. Des., vol. 123, pp. 99–110.

Shaw C.T., 1992, Using Computational Fluid Dynamics, Prantice Hall International (UK).

Tamburini A., Gentile L., Cipollina A., Micale G., and Brucato A., 2009. “Experimental investigation of dilute solid-liquid suspension in an unbaffled stirred vessels by a novel pulsed laser based image analysis technique,” Chem. Eng. Trans., vol. 17, pp. 531–536.

Tamburini A., Cipollina A., Micale G., Brucato A., and Ciofalo M., 2011. “CFD simulations of dense solid-liquid suspensions in baffled stirred tanks: Prediction of suspension curves,” Chem. Eng. J., vol. 178, pp. 324–341.

Tamburini A., Cipollina A., Micale G., Brucato A., and Ciofalo M., 2012a. “CFD simulations of dense solid-liquid suspensions in baffled stirred tanks: Prediction of the minimum impeller speed for complete suspension,” Chem. Eng. J., vol. 193–194, pp. 234–255.

Tamburini A., Cipollina A., Micale G., and Brucato A., 2012b. “Measurements of Njs and power requirements in unbaffled bioslurry reactors,” Chem. Eng. Trans., vol. 27.

Tamburini A., Cipollina A., Micale G., and Brucato A., 2013a. “Particle distribution in dilute solid liquid unbaffled tanks via a novel laser sheet and image analysis based technique,” Chem. Eng. Sci., vol. 87, pp. 341–358.

Tamburini A., Cipollina A., Micale G., Brucato A., and Ciofalo M., 2013b. “CFD simulations of dense solid-liquid suspensions in baffled stirred tanks: Prediction of solid particle distribution,” Chem. Eng. J., vol. 223, pp. 875–890.

Tamburini A., Brucato A., Busciglio A., Cipollina A., Grisafi F., Micale G., Scargiali F., and Vella G., 2014. “Solid-liquid suspensions in top-covered unbaffled vessels: Influence of particle size, liquid viscosity, impeller size, and clearance,” Ind. Eng. Chem. Res., vol. 53, no. 23.

Tamburini A., Cipollina A., Micale G., Scargiali F., and Brucato A., 2016. “Particle Suspension in Vortexing Unbaffled Stirred Tanks,” Ind. Eng. Chem. Res., vol. 55, no. 27, pp. 7535–7547.

Tamburini A., Gagliano G., Micale G., Brucato A., Scargiali F., and Ciofalo M., 2018. “Direct numerical simulations of creeping to early turbulent flow in unbaffled and baffled stirred tanks,” Chem. Eng. Sci., vol. 192, pp. 161–175.

Trad Z., Fontaine J. P., Larroche C., and Vial C.,2017. “Experimental and numerical investigation of hydrodynamics and mixing in a dual-impeller mechanically-stirred digester,” Chem. Eng. J., vol. 329, pp. 142–155.

Wang S., Parthasarathy R., Bong E. Y., Wu J., and Slatter P., 2012a. “Suspension of ultrahigh concentration solids in an agitated vessel,” AIChE J., vol. 58, no. 4, pp. 1291–1298.

Wang S., Boger D. V., and Wu J., 2012b. “Energy efficient solids suspension in an agitated vessel-water slurry,” Chem. Eng. Sci., vol. 74, pp. 233–243.

Wang S., Parthasarathy R., Wu J., and Slatter P., 2014. “Optimum solids concentration in an agitated vessel,” Ind. Eng. Chem. Res., vol. 53, no. 10, pp. 3959–3973.

Wilcox D. C., 1988. “Reassessment of the scale-determining equation for advanced turbulence models,” AIAA J., vol. 26, no. 11, pp. 1299–1310.

Yoshida M., Kimura A., Yoneyama A., and Tezura S., 2012. “Design and operation of unbaffled vessels agitated with an unsteadily forward-reverse rotating impeller handling solid-liquid dispersions,” Asia-Pacific J. Chem. Eng., vol. 7, no. 4, pp. 572–580.

Zamiri A. and Chung J. T., 2016. “Ability of URANS approach in prediction of unsteady turbulent flows in an unbaffled stirred tank,” Int. J. Mech. Sci., vol. 133, pp. 178–187.

Zhang P., Chen G., Duan J., and Wang W., 2018. “Mixing characteristics in a vessel equipped with cylindrical stirrer,” Results Phys., vol. 10, no. February, pp. 699–705.